Room Temperature Thermal Switching Based on Monolayer Boron Nitride

Dingbo Zhang(张定波)[1,2], Ke Wang(王珂)[3], Shuai Chen(陈帅)[4], Yuxiang Ni(倪宇翔)[1,2*], and Gang Zhang(张刚)[5*]

[1]*Key Laboratory of Advanced Technologies of Materials, Ministry of Education of China, School of Materials Science and Engineering, Southwest Jiaotong University, Chengdu 610031, China*
[2]*School of Physical Science and Technology, Southwest Jiaotong University, Chengdu 610031, China*
[3]*School of Automation, Xi'an University of Posts and Telecommunications, Xi'an 710121, China*
[4]*Materials Genome Institute, Shanghai Engineering Research Center for Integrated Circuits and Advanced Display Materials, Shanghai Frontier Science Center of Mechanoinformatics, Shanghai University, Shanghai 200444, China*
[5]*Yangtze Delta Region Academy of Beijing Institute of Technology (Jiaxing), Jiaxing 314019, China*

(Received 22 April 2025; accepted manuscript online 1 August 2025)

The research on materials capable of manipulating thermal conductivity continues to fuel the development of thermal controlling devices. Here, using *ab initio* calculations and the Boltzmann transport equation, we demonstrate that the thermal conductivity of semi-fluorinated hexagonal boron nitride (h-BN) can be reversibly manipulated at 300 K, and the ratio for the regulation of thermal conductivity reaches up to 11.23. Such behavior originates from the high sensitivity of thermal conductivity to magnetic ordering. Semi-fluorinated h-BN is a paramagnetic material at room temperature due to its Curie temperature of 270 K. Impressively, semi-fluorinated h-BN can be modulated into a ferromagnetic system by adding an external magnetic field of 11.15 T, resulting in greatly and reversibly tunable thermal conductivity at room temperature. Furthermore, in-depth analyses of phonon properties show that compared with the paramagnetic phase, both ferromagnetic and antiferromagnetic semi-fluorinated h-BN significantly reduce phonon scattering and anharmonicity, thereby enhancing thermal conductivity. The results qualify semi-fluorinated h-BN as a potential candidate for thermal switching applications at room temperature.

DOI: 10.1088/0256-307X/42/9/090603 CSTR: 32039.14.0256-307X.42.9.090603

1. Introduction. The thermal conductivity of two-dimensional (2D) materials has attracted worldwide attention for its critical role in understanding the fundamental principles and exploring advancements in various applications, including thermoelectric energy conversion and thermal controlling strategies.[1–5] In the past decades, different impacts on the thermal conductivity of 2D materials have been explored, including size effect,[6] substrate effect,[7] doping,[8] sample quality,[9] and strain.[10] Although great efforts have been made to tune the thermal conductivity of 2D materials, reversible and active manipulation of the thermal conductivity of 2D materials is still less explored.

In recent years, active regulation of thermal conductivity has continuously attracted increased research interest. Here, active regulation means that the thermal conductivity of the material can be actively controlled in the presence of an external field, such as an electric field or a magnetic field, and the thermal conductivity recovers its original value once the external field is removed. The advantage of active regulation compared with irreversible manipulation is obvious,[11] including dynamic manipulation of heat flux, thermal switching, and smart temperature management. As the magnetic ordering and other physical properties of 2D ferromagnetic materials are tunable under external fields (such as magnetic fields, electric fields, light fields, etc.), this provides a direct strategy for realizing a thermal switch. For example, for monolayer CrI_3,[12] $RuCl_3$,[13] $MnPS_3$,[14] and FeI_3,[15] at low temperatures around 20 K, thermal conductivity can be increased under external field effects. In a thermal switch, the major device performance factor is the switching ratio κ_{on}/κ_{off}, where κ_{on} (κ_{off}) is the thermal conductivity of the high (low) heat conductive state respectively. In addition to the switching ratio, high thermal conductivity is also preferred to obtain large thermal management ability. Unfortunately, in the aforementioned works,[12–15] either the switching ratio is low (less than 5), or the operating temperature is ultra-low (around 20 K) because of low magnetic phase transition temperatures. Moreover, the thermal conductivities of these samples are also low around their magnetic phase transition temperatures. These limit the application of 2D magnetic materials in active thermal regulation around room temperature.

Ultrahigh thermal conductivity was reported in graphene at room temperature, which provides a perfect testbed for studying phonon transport behavior in 2D systems.[16] Excluding graphene, hexagonal boron nitride (h-BN) has the highest room temperature thermal conductivity (1200 W/mK) among 2D materials.[9] More-

*Corresponding authors. Email: yuxiang.ni@swjtu.edu.cn; gangzhang2006@gmail.com
© 2025 Chinese Physical Society and IOP Publishing Ltd. All rights, including for text and data mining, AI training, and similar technologies, are reserved.

over, h-BN has a ∼6 eV bandgap distinct from that of graphene,[17] thus phonons are the dominant heat carriers in h-BN.[18] Due to the high thermal conductivity at room temperature, h-BN is widely believed to be a promising candidate for thermal management. However, pristine h-BN is a non-magnetic material; therefore, its thermal conductivity is insensitive to external fields. Interestingly, magnetism was successfully induced in the experiment by fluorinating h-BN.[19] In addition, control of the thermal conductivity of semiconductor fluorinated h-BN has not yet been studied.

In this work, from first-principles calculations, we found that semi-fluorinated h-BN is a ferromagnetic material with a Curie temperature around room temperature (270 K). Moreover, the ferromagnetic (FM), antiferromagnetic (AFM), and paramagnetic (PM) semi-fluorinated h-BN shows dramatically different thermal conductivities. Our work indicates that semi-fluorinated h-BN can be used as a high-performance thermal modulator by changing the magnetic ordering around room temperature.

2. Results.

2.1. The Geometrical Structures of Fluorinated h-BN. Figures 1(a)–1(e) display the structures of h-BN and four possible semi-fluorinated h-BN. According to the location of F atoms, we label the four possible semi-fluorinated h-BN as I (F on top of B), Ⅱ (F on top of N), Ⅲ (F on the hollow site), and Ⅳ (F in the middle of the bridge between B and N). Figure 1(f) shows the formation energy E_f assessed based on $E_f = (E_{\text{F-BN}} - E_{\text{BN}} - \mu_F)/N_F$, where $E_{\text{F-BN}}$ and E_{BN} are the total energies of optimized semi-fluorinated h-BN and h-BN, respectively. μ_F and N_F are the chemical potential and number for the adsorbed F atoms, respectively. $\mu_F = -4.98$ eV. Structure I is most stable with $E_f = -0.30$ eV, while structures Ⅱ and Ⅲ are unstable due to their positive formation energies. After geometric relaxation, structure Ⅳ transforms into structure I, indicating that this structure does not exist. In addition, *ab initio* molecular dynamics (AIMD) simulations were performed using the canonical ensemble (NVT) at 270 K. The AIMD simulation results show that only the energy of structure I fluctuated slightly around a certain value (−313.5 eV), and its structure, bond lengths, and bond angles did not change significantly compared with those of the corresponding original unit cell [see Fig. S1 in the Supplementary Materials (SM)]. Thus, we focus on structure I for semi-fluorinated h-BN in the following sections.

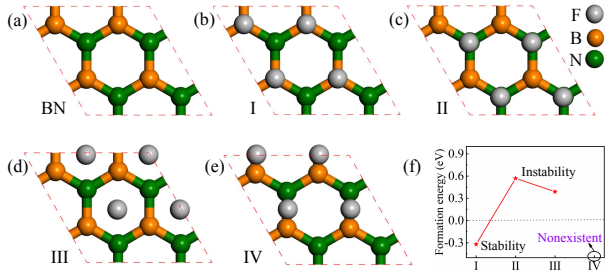

Fig. 1. The possible structures of fluorinated h-BN. (a) The structure of h-BN. (b)–(e) Four possible adsorption structures of semi-fluorinated h-BN. (f) The formation energies.

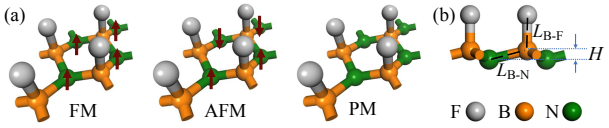

Fig. 2. The magnetic structures of semi-fluorinated h-BN. (a) Perspective and (b) side views of semi-fluorinated h-BN with the FM/AFM/PM magnetic ordering.

When spin is introduced to semi-fluorinated h-BN, the magnetic moment of the N atoms is about 1 μ_B, whereas that of the B and F atoms is negligible (<0.01 μ_B). The underlying physical mechanism can be explained as follows: the semi-fluorination induces a change in the electron orbital of a B atom from sp^2 to sp^3 hybridization, which prevents the charge transfer from N to B atoms. As a result, $2p_z$ electron on N atoms is not paired, and the extended $2p_z$–$2p_z$ orbital interaction causes long-range magnetic ordering.[19]

To study the magnetic state of semi-fluorinated BN, the corresponding FM, AFM, and PM phases were considered as plotted in Fig.2. The total energy of the FM phase is −78.75 eV, which is 0.13/2.19 eV lower than that in the AFM/PM phases, suggesting that semi-fluorinated h-BN is an FM material at temperatures below the Curie temperature. Based on mean field theory (MFT) considering the energy difference between FM and AFM states,[20,21] the Curie temperature T_C^{MFT} of semi-fluorinated h-BN is estimated to be 270 K by using the corresponding expression: $T_C^{\text{MFT}} = \frac{2}{3}\frac{E_{\text{AFM}} - E_{\text{FM}}}{k_B c}$, where k_B is the Boltzmann constant and c is the concentration of magnetic atoms. Moreover, the FM semi-fluorinated h-BN can be transformed into an AFM phase by applying in-plane strain because the energy difference between AFM and FM states decreases as compressive strain increases. At 3% compression, the AFM state is energetically more stable than its FM counterpart (Fig. S2 in the SM), indicating that a compression rate of 3% can induce a magnetic transition from the FM state to the AFM state. The corresponding phase transition mechanism can be understood as strain-induced reversal of the spin vector on p_z orbital of N atom, as illustrated in Fig. S3 of the SM.

As shown in Table 1, the lattice parameters and B-N bond lengths for the FM/AFM/PM phases are 5.29/5.28/5.26 Å and 1.57/1.57/1.56 Å, respectively. These results indicate that spin induces an increment in the lattice constant and B-N bond length, which is consistent with previous reports.[22,23] On the contrary, the B-F bond length is slightly reduced in FM (1.41 Å) and AFM (1.40 Å) states compared with that in PM (1.42 Å) state. The planar structure in h-BN bears a buckling structure by absorbing F atom, leading to a vertical height H between planes of B and N atoms. The H of FM/AFM phases is 5.71% higher than that of the PM phase. The spin-induced structural changes are directly reflected in the electronic projected density of states (ePDOS) (Fig. S3 in the SM). Based on the ePDOS, the overlap of electronic orbits in the FM/AFM/PM phases was evaluated by computing covalency between different atoms, which is directly proportional to phonon anharmonicity.[12] The order of absolute values of covalency (Table S1 in the SM) between

Table 1. Relative energies (E), lattice parameters, B-F and B-N bond lengths ($L_{\text{B-F}}$ and $L_{\text{B-N}}$), vertical B-N plane heights (H), and magnetic moments (M) in $2 \times 2 \times 1$ supercells of FM/AFM/PM phases are presented. The energy of the FM phase was set to zero, as its total energy is the lowest.

Magnetic ordering	E (eV)	Lattice parameters (Å)	$L_{\text{B-F}}$ (Å)	$L_{\text{B-N}}$ (Å)	H (Å)	M (m_{B})
FM	0.00	5.29	1.41	1.57	0.37	4.00
AFM	0.13	5.28	1.40	1.57	0.37	0.00
PM	2.19	5.26	1.42	1.56	0.35	4.00

individual pairs of atoms is FM < AFM < PM, which implies that FM/AFM semi-fluorinated h-BN structures bear lower phonon anharmonicity than PM phase.

2.2. The Magnetic Ordering-Dependent Phonon Properties of Fluorinated h-BN. To distinguish the impact of magnetic ordering on the phonon properties, we calculated the phonon dispersion of FM/AFM/PM semi-fluorinated h-BN, as exhibited in Fig. 3(a). No imaginary frequencies emerge in the phonon spectrum, which implies thermodynamics stability of these structures.

The phonon dispersion curves of AFM and FM phases have analogous shapes, but notable shifts in frequency for the same lattice vibration mode. In addition, the phonon dispersion of the PM phase is distinct from that of the other two phases. The symmetry of semi-fluorinated h-BN causes five Raman-active phonon modes,[24] and we perform an in-depth analysis for the two most easily discernible patterns: A_1 and E modes. Their vibration eigenvectors are shown in the inset of Fig. 3(b). All atoms in A_1 (E) mode undergo an in-plane (out-of-plane) motion. As exhibited in Fig. 3(b), the frequencies of A_1 and E modes of semi-fluorinated h-BN are 6.696 THz and 21.342 THz at Γ point in the PM phase, while these values are 3.649 (6.452) THz and 21.808 (21.821) THz in the FM (AFM) phase, respectively. The frequency difference is attributed to the different magnetic exchange interactions among the three semi-fluorinated h-BN.

The magnetic ordering-dependent phonon properties are analyzed by exploring the harmonic interatomic force constants (IFCs). Based on the frozen magnon method,[25] the relationship of the harmonic IFCs between FM (AFM) and PM structures is described by the following formula:

$$\tilde{F}_{\boldsymbol{R}i\alpha\boldsymbol{R}'j\beta} = F_{\boldsymbol{R}i\alpha\boldsymbol{R}'j\beta} - \sum_{mn} J''_{\boldsymbol{R}i\alpha\boldsymbol{R}'j\beta;mn}\langle \boldsymbol{S}_m \cdot \boldsymbol{S}_n \rangle, \quad (1)$$

where $\tilde{F}$ and F are the harmonic IFCs in FM (AFM) and PM phases, respectively. J'' stands for the second derivative of magnetic exchange interaction J. The movement of atom i is marked by $\boldsymbol{R}$ ($\boldsymbol{R}'$) lattice vector along the α (β) Cartesian direction. The first nearest-neighbor atoms interaction was considered due to the huge spin dynamics in magnetic semi-fluorinated h-BN. Thus, the J'' of FM and AFM phases are obtained via $\tilde{F}_{\text{FM}} = F - 6J''S^2$ and $\tilde{F}_{\text{AFM}} = F + 6J''S^2$, respectively. S is equal to half of the spin number in a magnetic atom. As plotted in Fig. S4 of the SM, most of the out-of-plane (ZZ) components of J'' are much lower than the in-plane (XX and YY) components in both FM and AFM phases, demonstrating that the magnetic exchange interaction mainly exists in the in-plane direction. Therefore, compared with out-of-plane phonon modes, the in-plane phonon modes are more sensitive to magnetic ordering.

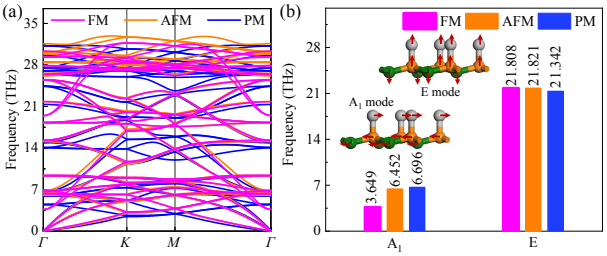

Fig. 3. The phonon properties of fluorinated h-BN. (a) The phonon dispersions with the non-analytical term correction. (b) The phonon frequencies of A_1 and E Raman-active modes of semi-fluorinated h-BN with FM/AFM/PM ordering. The inset in (b) presents vibration eigenvectors for A_1 and E modes.

2.3. Magnetic Ordering-Controllable Thermal Conductivity. In this section, we investigate the magnetic ordering-dependent thermal conductivities of semi-fluorinated h-BN. To verify the reliability of our calculations, the thermal conductivity of pure h-BN was calculated (as shown in Fig. S5 of the SM), which is consistent with the previously reported value (1134 W/mK at 300 K).[26] We then computed the temperature-dependent thermal conductivities of semi-fluorinated h-BN with FM/AFM/PM ordering [Fig. 4(a)], all of which are lower than that of intrinsic h-BN. Analogous results were reported in fluorinated Sn_2Bi.[27]

Around the Curie temperature (270 K), with temperature increasing or decreasing, the FM-PM or PM-FM magnetic phase transition will result in a large change in thermal conductivity (from 74.75 W/mK to 6.53 W/mK or reversely). In addition to the temperature-controlled thermal regulation, the thermal conductivity of semi-fluorinated h-BN can also be actively controlled by a magnetic field. Semi-fluorinated h-BN possesses a PM state at room temperature because its Curie temperature is 270 K. The reversible regulation of the magnetic ordering of semi-fluorinated h-BN can be realized by applying or removing the external magnetic field, resulting in reversibly tunable thermal conductivity. In the Heisenberg spin model (see details in the SM), when temperature T is higher than the Curie temperature T_{C}, the magnetic field B_Z required to preserve the FM state is

$$g\mu_{\text{B}}B_Z \geq (T - T_{\text{C}})k_{\text{B}}, \quad (2)$$

where g is the spin g-factor, μ_{B} is the Bohr magneton, and B_Z is the strength of the magnetic field. Using the parameters of semi-fluorinated h-BN, we find that by applying an external magnetic field of 11.15 T perpendicular to the h-BN layer, semi-fluorinated h-BN is in a FM state at 300 K. Such a magnetic field is experimentally achievable, as an external magnetic field around 10 T

was used to modulate the magnetic ordering of 2D magnetic materials ($MnPS_3$ [28] and $CrCl_3$ [15]). As shown in Fig. 4(b), the thermal conductivities of semi-fluorinated h-BN with FM and PM ordering are 71.96 and 6.41 W/mK at 300 K, respectively. Therefore, a tenfold thermal conductivity increase can be realized in semi-fluorinated h-BN at room temperature with reasonable magnetic field strength. This thermal switch ratio is significantly higher than that of almost all previously reported 2D magnetic materials, such as semi-hydrogenated graphene (2.27) [24] and 2D iron and ruthenium trihalides (1.31–5.73). [15] Although CrI_3 has a thermal conductivity modulation ratio of 15.03, it has a very low room temperature thermal conductivity (0.033/0.496 W/mK for the PM/FM phases). [12]

In addition to temperature-driven and magnetic field-driven thermal regulation, below the Curie temperature (270 K), only a 3% compression strain can result in an FM-AFM magnetic phase transition, associated with an 18.32% reduction in the thermal conductivity of semi-fluorinated h-BN. Therefore, semi-fluorinated h-BN has significant advantages as a critical part of thermal switching devices compared with all previously reported 2D ferromagnets.

It can be found from Fig. 4(c) that different magnetic ordering slightly affects the contribution of ZA phonons to the thermal conductivity. On the other hand, magnetic ordering has a pronounced effect on that of in-plane (TA and LA) acoustic phonons, which agrees with the above calculation of harmonic IFCs. Compared with FM ordering, the contribution from optical phonons to the thermal conductivity of AFM and PM phases is obviously reduced, which is one of the origins of reduced thermal conductivity. To comprehensively reveal the effect of magnetic ordering on the thermal conductivity of semi-fluorinated h-BN, we explored the corresponding phonon characteristics. For FM/AFM/PM semi-fluorinated h-BN, the group velocities of the acoustic phonon branches are approximately similar to each other; only optical phonon modes in FM state have higher values of group velocity (Fig. S6 in the SM). Thus, the change in optical phonon group velocity has a small contribution to large magnetic-driven thermal regulation.

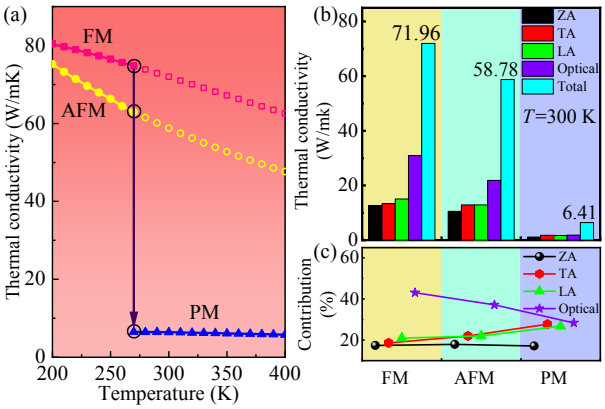

Fig. 4. The thermal conductivities of fluorinated h-BN. (a) The magnetic ordering-dependent thermal conductivities of semi-fluorinated h-BN. (b) The thermal conductivities of three acoustic modes (ZA: out-of-plane acoustic, TA: transverse acoustic, and LA: longitudinal acoustic) and optical phonon modes in the three phases at room temperature. (c) The corresponding contribution of these modes.

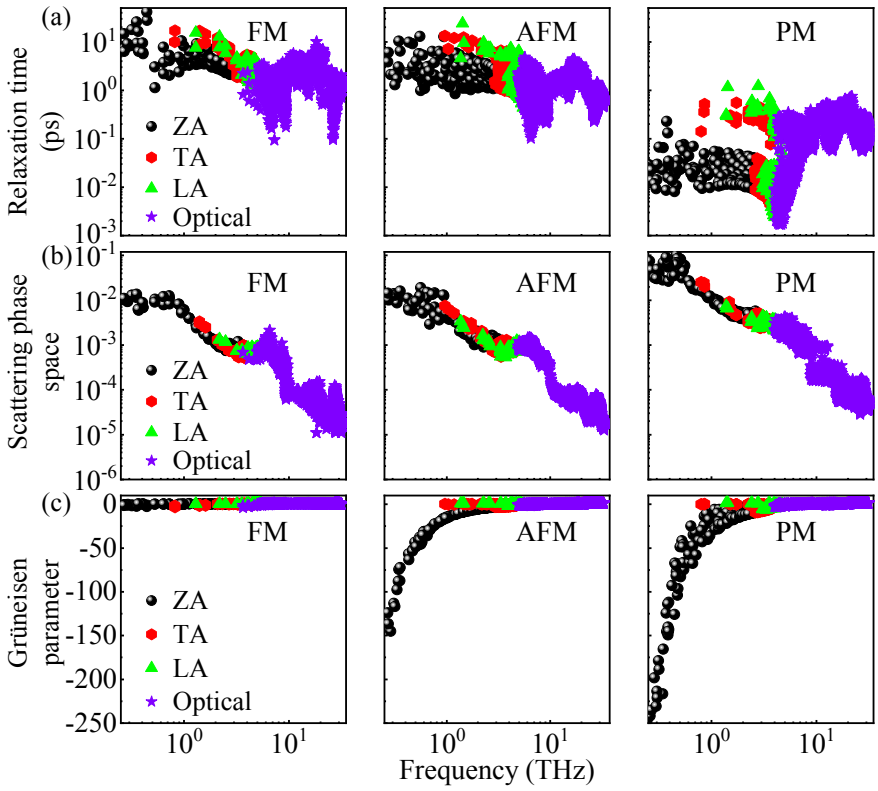

Fig. 5. The phonon characteristics of semi-fluorinated h-BN. (a) Phonon relaxation time. (b) Scattering phase spaces. (c) Grüneisen parameters of semi-fluorinated h-BN with FM/AFM/PM ordering.

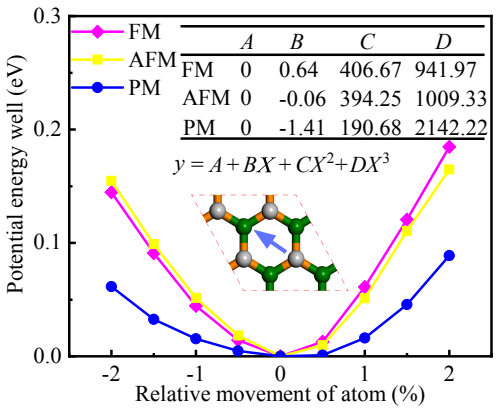

Fig. 6. The potential-energy well of semi-fluorinated h-BN. The potential energy curves for the FM/AFM/PM semi-fluorinated h-BN are shown in pink, yellow, and blue.

The magnetic ordering-dependent phonon relaxation time of semi-fluorinated h-BN is presented in Fig. 5(a). Compared with the PM phase, there is a 2–3 orders of magnitude enhancement in phonon relaxation time in FM/AFM phases, revealing the largely suppressed phonon scattering possibility. The scattering phase spaces among the three phases are almost similar, as shown in Fig. 5(b). The only difference is that over the whole frequency range, the scattering phase spaces of the FM/AFM phases are slightly lower than that of the PM phase, which implies smaller phonon–phonon scattering channels in FM/AFM semi-fluorinated h-BN. As the scattering phase space is described by the conservation of energy and momentum of the phonon modes involved, its variation with frequency is consistent with the phonon branch density in phonon dispersion.[29–31] However, the phonon scattering phase space changes only slightly among the three phases, which cannot fully explain the greatly enhanced phonon relaxation time. Next, we explored the Grüneisen parameter, as presented in Fig. 5(c). The absolute values of average Grüneisen parameter for FM, AFM, and PM phases are 0.17, 0.31, and 0.54, respectively. Consequently, both FM and AFM magnetic orderings remarkably reduce photon scattering and anharmonicity compared to PM ordering; this accordingly changes thermal conductivity of semi-fluorinated h-BN.

Figure 6 presents the potential-energy well of semi-fluorinated h-BN with FM/AFM/PM ordering, providing another perspective to understand the magnetic ordering-dependent phonon anharmonicity. The potential-energy wells were fitted by a polynomial to obtain C (harmonic parameters) and D (anharmonic parameters),[32] as listed in the table of Fig. 6. The small increase in C for the FM/AFM phases reveals a slightly enhanced bonding strength (Table 1) and a little change in group velocity (Fig. S6 in the SM). The largely reduced D in the FM/AFM phases reveals that phonon anharmonicity is significantly weakened, which is consistent with the results for the Grüneisen parameter above.

3. Conclusion. In this work, we report the most stable semi-fluorinated h-BN structure whose thermal conductivity can be reversibly manipulated (10-fold) at room temperature. FM and AFM magnetic states can be mutually converted via strain. Moreover, we found that by applying an external magnetic field of 11.15 T, the FM state can be preserved in semi-fluorinated h-BN at room temperature. The thermal conductivity of the FM (AFM) semi-fluorinated h-BN is 11.23 (9.12) times that of the PM phase at 300 K. Analyses of the phonon behaviors demonstrate that the FM/AFM phases have larger thermal conductivities than the PM phase due to longer phonon relaxation time, smaller scattering phase spaces, and attenuation of phonon anharmonicity. This work provides a possibility for a 2D thermal modulator which can be applied in active and reversible heat flow control.

4. Methods. First-principle calculations in our work were carried out using the Vienna *ab initio* simulation (VASP) package,[33] within the Perdew–Burke–Ernzerh exchange-correlation functional.[34] During the structural optimization, electronic property calculations, and thermal conductivity analysis, the convergence criteria for electronic relaxation is 10^{-7} eV and for ionic relaxation is 10^{-3} eV/Å. The cutoff energy is 600 eV and the K-mesh is $25 \times 25 \times 1$. Calculations of the second-order force constants were performed via Phonopy.[35] By using third-order and fourth-order codes, we calculated the third-order and fourth-order force constants, respectively. The thermal conductivity was calculated based on ShengBTE[36] and Fourphonon.[37] In the calculations of phonon dispersion and thermal conductivity, we also took into account the non-analytical term correction. Detailed methods are given in the SM.

Data Availability. The authors declare that all data supporting the findings of this study are available in the manuscript and SM. Additional data from the authors can be provided upon request.

Acknowledgements. This work was supported by the Postdoctoral Fellowship Program (Grade C) China Postdoctoral Science Foundation (Grant No. GZC20241421), the Sichuan Science and Technology Program (Grant No. 2025ZNSFSC0864), and the Fundamental Research Funds for the Central Universities (Grant No. 2682025CX029).

References

[1] Qian X, Zhou J W, and Chen G 2021 *Nat. Mater.* **20** 1188
[2] Gu X K, Wei Y J, Yin X B, Li B W, and Yang R G 2018 *Rev. Mod. Phys.* **90** 041002
[3] Marconnet A M, Panzer M A, and Goodson K E 2013 *Rev. Mod. Phys.* **85** 1295
[4] Song H F, Liu J M, Liu B L, Wu J Q, Cheng H M, and Kang F Y 2018 *Joule* **2** 442
[5] Balandin A A 2011 *Nat. Mater.* **10** 569
[6] Zhang Z W, Ouyang Y L, Cheng Y, Chen J, Li N B, and Zhang G 2020 *Phys. Rep.* **860** 1
[7] Sadeghi M M, Jo I, and Shi L 2013 *Proc. Natl. Acad. Sci. U.S.A.* **110** 16321
[8] Wang X W, Sun G Z, Routh P, Kim DH, Huang W, and Chen P 2014 *Chem. Soc. Rev.* **43** 7067
[9] Cai Q R, Scullion D, Gan W, Falin A, Zhang S Y, Watanabe K J, Taniguchi T, Chen Y, Santos E J, and Li L H 2019 *Sci. Adv.* **5** eaav0129
[10] Cheng Y, Wu X, Zhang Z J, Sun Y, Zhao Y S, Zhang Y Y, and Zhang G 2021 *Nanoscale* **13** 1425

[11] Wehmeyer G, Yabuki T, Monachon C, Wu J, and Dames C 2017 *Appl. Phys. Rev.* **4** 041304
[12] Qin G Z, Wang H M, Zhang L C, Qin Z Z, and Hu M 2020 *J. Mater. Chem. C* **8** 3520
[13] Yu Y J, Xu Y, Ran K J, Ni J M, Huang Y Y, Wang J H, Wen J S, and Li S Y 2018 *Phys. Rev. Lett.* **120** 067202
[14] Zhang D B, Wang K, Chen S, Zhang L F, Ni Y X, and Zhang G 2023 *Nanoscale* **15** 1180
[15] Liu Y Q, Liu Q X, Liu Y, Jiang X, Zhang X L, and Zhao J J 2021 *Nanoscale* **13** 7714
[16] Wu R, Zhu R Z, Zhao S H, Zhang G, Tian H, and Ren T L 2021 *Sci. China Inf. Sci.* **64** 140401
[17] Wang J G, Ma F C, Liang W J, and Sun M T 2017 *Mater. Today Phys.* **2** 6
[18] Zhao Y S, Cai Y Q, Zhang L F, Li B W, Zhang G, and Thong J T 2020 *Adv. Funct. Mater.* **30** 1903929
[19] Radhakrishnan S, Das D, Samanta A, de Los Reyes C A, Deng L, Alemany L B, Weldeghiorghis T K, Khabashesku V N, Kochat V, and Jin Z 2017 *Sci. Adv.* **3** e1700842
[20] Zhou J, Wang Q, Sun Q, Chen X, Kawazoe Y, and Jena P 2009 *Nano Lett.* **9** 3867
[21] Penny C, Muxworthy A R, and Fabian K 2019 *Phys. Rev. B* **99** 174414
[22] Zhou J, Wang Q, Sun Q, and Jena P 2010 *Phys. Rev. B* **81** 085442
[23] Kan E J, Xiang H J, Wu F, Tian C, Lee C, Yang J, and Whangbo M H 2010 *Appl. Phys. Lett.* **97** 122503
[24] Li H Q, Zhang P, Ouyang T, Wang H M, Li J, He C Y, Zhang C X, and Tang C 2022 *Appl. Phys. Lett.* **120** 092403
[25] Pandey T, Peeters F M, and Milošević M V 2021 *2D Mater.* **9** 015034
[26] Fan H, Wu H, Lindsay L, and Hu Y J 2019 *Phys. Rev. B* **100** 085420
[27] Li T W, Yu J B, Nie G, Zhang B P, and Sun Q 2020 *Nano Energy* **67** 104283
[28] Long G, Henck H, Gibertini M, Dumcenco D, Wang Z, Taniguchi T, Watanabe K, Giannini E, and Morpurgo A F 2020 *Nano Lett.* **20** 2452
[29] Lindsay L, Broido D A, and Mingo N 2011 *Phys. Rev. B* **83** 235428
[30] Zhang D B, Hu S, Sun Y J, Liu X, Wang H, Wang H Y, Chen Y Z, and Ni Y X 2020 *ES Energy & Environment* **10** 59
[31] Zhang D B, Hu Y, Zhong H X, Yuan S J, and Liu C 2019 *Nanoscale* **11** 13800
[32] Qin G Z, Qin Z Z, Wang H M, and Hu M 2018 *Nano Energy* **50** 425
[33] Hafner J 2008 *J. Comput. Chem.* **29** 2044
[34] Ernzerhof M and Scuseria G E 1999 *J. Chem. Phys.* **110** 5029
[35] Togo A and Tanaka I 2015 *Scripta Mater.* **108** 1
[36] Li W, Carrete J, Katcho N A, and Mingo N 2014 *Comput. Phys. Commun.* **185** 1747
[37] Han Z R, Yang X L, Li W, Feng T L, and Ruan X 2022 *Comput. Phys. Commun.* **270** 108179